# Dynamics of Polymer Melts above the Glass Transition: Monte Carlo Studies of the Bond Fluctuation Model

**K. Okun, M. Wolfgardt, J. Baschnagel,† and K. Binder***

*Institut für Physik, Johannes Gutenberg-Universität Mainz, Staudingerweg 7, D-55099 Mainz, Germany*

*Received October 29, 1996; Revised Manuscript Received February 25, 1997*[⊗]

ABSTRACT: The bond fluctuation model on the simple cubic lattice with a bond-length dependent potential energy favoring long bonds exhibits a glassy freezing in as the temperature is lowered, many properties being qualitatively similar to experiment. The present paper studies the dynamical properties of the model (as they result from the "random hopping" algorithm), using configurations of undercooled polymer melts that have been carefully equilibrated by the "slithering snake" algorithm. In this way quantitatively reliable data can be obtained for distinctly lower temperatures than in the previous work on the dynamics of this model that used the random hopping algorithm for equilibration as well. If various mean-square displacements, the self-diffusion constant, autocorrelation functions of the end-to-end vector, intermediate incoherent scattering functions, and single chain dynamic structure factors are analyzed, it is found that the slowing down of relaxation times occurs according to the Vogel−Fulcher law. Within the uncertainties of the analysis the Vogel−Fulcher temperature of all these times is the same, $0.12 \leq T_0 \leq 0.13$. Particularly illuminating is an analysis of the Rouse modes, which supports this conclusion and furthermore yields compelling evidence for the time−temperature superposition principle. It is shown that no static cross-correlations develop between different Rouse modes in the undercooled melt.

## I. Introduction

Understanding the glass transition of polymer melts (and other glass-forming undercooled fluids) is still a particular challenge.[1−6] The information about structure that results from elastic diffuse scattering of X-rays or neutrons shows only small differences between the supercooled polymer melt and the glass, although the dynamical properties are very different. Remarkable qualitative similarities in the behavior of chemically very different polymers (and even non-polymeric systems[1−6]) also occur. Also the physical mechanisms that can explain ubiquitous features of glassy relaxation (e.g. the Vogel−Fulcher "law"[7] describing the increase of the relaxation times near the glass transition, the Kohlrausch−Williams−Watts "law"[8] describing the stretching of relaxation functions, and scaling ideas like the time−temperature−superposition principle[2]) remain somewhat controversial.

In this situation the study of the glass transition by computer simulation seems very attractive, since computer simulations yield arbitrarily detailed information about both static and dynamic properties of model systems.[9−13] However, flexible polymer chains of large molecular weight exhibit static structure from the bond length (1 Å), to the coil size (100 Å), and motions occur on the scale of $10^{-14}$ s (bond length vibrations) to $10^{-5}$ s (relaxation time of the global coil configuration), even at temperatures far above the glass transition.[12,14,15] This enormous spread of both length scales and time scales makes the fully atomistic simulation of polymeric materials extremely difficult,[12,14,15] and full thermal equilibrium can only be reached for relatively short chains of rather simple chemical architecture at fairly high temperature, such as, e.g., polyethylene $C_{100}H_{202}$ at 509 K.[16−18] A simulation of glassification of such melts is only possible in the framework of extremely rapid quenches,[19−21] whose time constant is much smaller than the single-chain Rouse time at high temperatures. Although sometimes the view has been expressed that all what rapid quenching does is to shift the glass transition temperature $T_g$ to higher temperatures,[21,22] there now is ample evidence (for spin glasses,[23] orientational glasses,[24] and structural glasses such as undercooled Lennard−Jones mixtures[25] or $SiO_2$[26]) that both local and global physical properties depend distinctly on the cooling rate. Hence no reliable conclusions can be drawn from rapid quenching simulations on the physical characteristics of the glass transition of a fluid which is cooled very slowly and thus held nearly in metastable equilibrium. It is the latter situation, of course, that is exclusively considered by the theories that one wishes to test.[1−5,27−33]

Thus the bond fluctuation model[34−36] has been proposed as a coarse-grained model describing[37−44] the glassy freezing in of polymer melts. In this model, effective monomers that block the eight sites of an elementary cube of the lattice for further occupation are connected by effective bonds that can vary in bond length from $2 \leq b \leq \sqrt{10}$ (all lengths being measured in units of the lattice spacing). If an effective bond is interpreted as a kind of Kuhn segment formed from n successive chemical bonds along the backbone of the chain ($n \approx 3-5$),[15,45] the "random hopping" algorithm where a monomer moves by one lattice unit in a randomly chosen lattice direction (provided this move complies with excluded volume and bond length constraints) models the random configurational changes of such Kuhn segments effected via jumps over barriers of the torsional potential.[15,45,46] Disposing of the fast vibrational motions of bond lengths and bond angles, and of the small scale local structure, one considerably gains in computational efficiency[37,44] (on the order of $10^6$ attempted monomer moves are carried out per CPU second). It has been estimated that near $T_g$ a time window from about $10^{-12}$ s to $10^{-5}$ s becomes accessible.[15,46] A glass transition is produced in the model by introducing a Hamiltonian for the bond vector $H(\vec{b})$

† Present address: Institut Charles Sadron, 6, rue Boussingault, F-67083 Strasbourg Cedex, France.

[⊗] Abstract published in *Advance ACS Abstracts,* April 15, 1997.

S0024-9297(96)01605-1 CCC: $14.00 

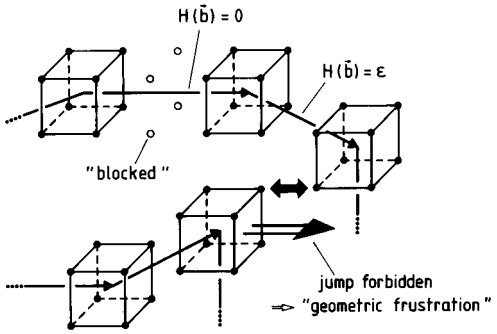


**Figure 1.** Sketch of a possible configuration of effective monomers belonging to different chains in the melt in order to illustrate the effect of the energy function $H(\vec{b})$. All bond-vectors $b$ have the energy $H(\vec{b}) = \epsilon$ (=1 in our units) except $b_0 = (\pm 3,0,0)$ {or permutations thereof} for which $H(\vec{b}) = 0$. However, this vector "blocks" four sites (marked by white circles) for further occupation, since two monomers may not overlap. E.g., due to this excluded volume interaction, the jump indicated by the large arrow is forbidden. As more and more bonds take their ground state $b_0$, more and more free volume is wasted by the blocked sites, and in a dense polymer melt for some bonds it becomes impossible to reach their ground state due to these constraints in their neighborhood. This "geometric frustration" leads to glassy behavior. Figure modified from Baschnagel et al.[39]

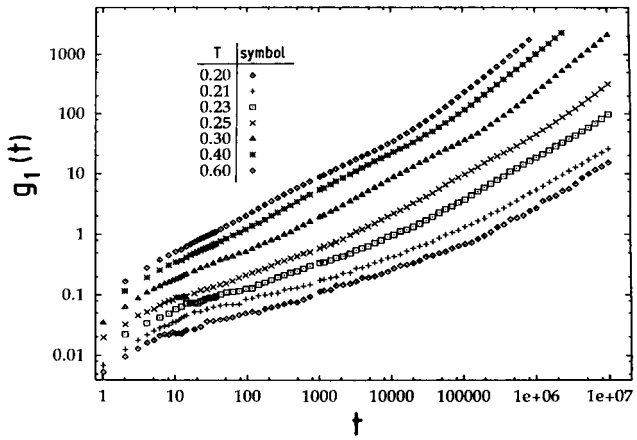


**Figure 2.** Log−log plot of the mean-square displacements of inner monomers $g_1(t)$ vs time $t$, for chains of length $N = 10$ and a volume fraction $\phi = 0.533$ of occupied sites, at seven temperatures from $T = 0.60$ (top curve) to $T = 0.2$ (bottom curve), as indicated by different symbols. Note that at each temperature (measured in units of $\epsilon = 1$, note $k_B \equiv 1$) the initial state at time $t = 0$ was obtained from configurations carefully equilibrated with the slithering snake algorithm. All data are for $30 \times 30 \times 30$ lattices with periodic boundary conditions. Time is measured in units of attempted Monte Carlo steps per monomer (MCS).

that favors long bonds:[39] $H(\vec{b}) = 0$ if $\vec{b} = (\pm 3,0,0)$ or a permutation thereof; $H(\vec{b}) = \epsilon = 1$ otherwise (Figure 1).

We work at a volume fraction of $\phi = 8NP/L^3 = 0.5333$ occupied sites, with chain length $N = 10$, number of polymers $P = 180$, and lattice linear dimension $L = 30$. This choice corresponds to the case of dense melts, as shown elsewhere.[36,39,40] In order to sample enough different typical configurations to be really representative of a macroscopic system, 16 completely independent "replicas" of the system are averaged over.

Nevertheless, these time scales available in the model are still orders of magnitude smaller than the time scales accessible in the experiment, and thus one must expect that the effects of (relatively) fast cooling rates will still hamper the observation of physical properties in the simulation model. This expectation has been proven[39] in simulations where the cooling rate was varied over several orders of magnitude (although the time constants of these cooling rates were much larger than the Rouse time of the chains at high temperatures, using extremely short chains of $N = 10$ effective monomers only).

Recently it was shown that progress can be obtained[42,45] using dynamical Monte Carlo algorithms with unphysical moves such as the "slithering snake" algorithm[46,47] to equilibrate the configurations of the undercooled polymer melt. One can win about 3 orders of magnitude in the relaxation time[42,45] and generate thus rather well-equilibrated melt configurations closer to the glass transition temperature than with the "random hopping" algorithm itself. In the present paper, we hence reconsider the dynamics of such models for undercooled polymer melts, using the slithering snake algorithm for the generation of starting configurations, which are then used for runs applying the "random hopping" algorithm to investigate dynamical properties of such states. Of course, at temperatures high enough that "random hopping" can equilibrate the system, runs with the slithering snake algorithm and with random hopping give identical results for the static properties, as has been discussed in detail elsewhere.[42]

In section II we shall present our resulting data for the mean-square displacements of inner monomers and of the center of gravity, discuss the resulting effective mobility $W(T)$ and self-diffusion constant $D(T)$, and analyze also the correlation functions of the end-to-end vector. Dynamic structure factors are presented in section III, while an analysis of chain dynamics in terms of Rouse modes is given in section IV. Finally, section V summarizes our conclusions.

## II. Mean Square Displacements and Time-Dependent Correlation Functions

Figure 2 shows a log−log plot of the mean-square displacement $g_1(t)$ of inner monomers vs time

$$g_1(t) \equiv \langle [\vec{r}_n(t) - \vec{r}_n(t=0)]^2 \rangle \tag{1}$$

Here $\langle ... \rangle$ stands for an average over the two innermost monomers $n$ of each chain (chain length $N = 10$), over all polymers in the simulated system, and over 16 independent configurations. Thus the statistics of $g_1(t)$ is based on an average over 5760 effective monomers.

The data of Figure 2 extend over 7 decades in time and allow one to distinguish several regimes. In the time interval $1 \le t \le 10$ MCS the increase of $g_1(t)$ with $t$ is relatively fast, and the slope in this regime is not strongly temperature dependent. In the regime from about $t \approx 10$ MCS to the chain relaxation time $\tau$ (defined e.g. by the condition that $g_1(t = \tau) = \langle R^2 \rangle$, the mean-square end-to-end distance of the chain) the increase of $g_1(t)$ with $t$ is clearly subdiffusive, $g_1(t) \propto t^{x_1}$ ($x_1 < 1$), and the (effective) exponent $x_1$ clearly decreases with decreasing temperature. At times $t > \tau$, one has a simple diffusive behavior

$$g_1(t) = 6Dt, \quad t > \tau \tag{2}$$

where $D$ is the self-diffusion constant of the chains.

For non-entangled chains (note that $N = 10$ is about four times smaller than the entanglement chain length) at times $t < \tau$, the Rouse model[48,49] predicts a simple diffusion on the scale of the effective segment length $l$ (which is of the same order as $\langle b^2 \rangle^{1/2}$)

$$g_1(t) \propto l^2(Wt), \quad g_1(t) < l^2 \text{ or } t < 1/W \tag{3}$$

where $W$ is a rate describing the jumps of the effective monomers per unit time, while subdiffusive behavior is predicted at later times

$$g_1(t) \propto l^2(Wt)^{1/(1+1/2\nu)}, \quad l^2 < g_1(t) < \xi^2 \tag{4}$$

$$g_1(t) \propto \xi^2(l/\xi)^{1+1/2\nu}\,(Wt)^{1/2}, \quad \xi^2 < g_1(t) < \langle R^2\rangle \tag{5}$$

where $\xi$ is the screening length of excluded volume interactions.[36,50] Since in dense melts $\xi$ and $l$ are of the same order of magnitude, the observability of the regime described by eq 4 is very much restricted. In addition, an inspection of Figure 2 shows that (i) the crossover from eq 3 to a slower relaxation already occurs for mean-square displacements $g_1(t)$ on the order of 0.1, i.e. much smaller mean-square displacements than $\langle b^2\rangle$, and (ii) the exponent $x_1$ in the law $g_1(t) \propto t^{x_1}$ is compatible with eqs 4 or 5 only at rather high temperatures, while for $T \leq 0.3$ effective exponents $x_1(T) < {}^1/_2$ are obtained. The smallness of these effective exponents also reflects the "cage effect"[5,27]—the diffusion of the monomers is strongly hindered by their environment. On the basis of Figure 2 one can already conclude that for an undercooled melt the Rouse model in its standard simple form does not hold, because eq 5 is not verified. In section IV we shall see, however, that a generalized type of Rouse dynamics still holds, with Rouse modes that show stretched exponential decay rather than the standards simple exponential decay.[49]

In view of the fact that none of eqs 3−5 is clearly seen in the log−log plot in Figure 2, the estimation of the rate factor $W(T)$ is not straightforward. We thus have tentatively considered plots of $g_1(t)$ vs $t^{1/(1+1/2\nu)} = t^{0.54}$, since in these plots one can find significantly large regions in time where $g_1(t)$ can be described as a straight line with a nonzero intercept, i.e. $g_1(t) = m(T)t^{0.54} + n(T)$, where $m(T)$ is some effective mobility and the intercept $n(T)$ accounts for the fact that for very short times ($t \leq$ 10 MCS) a faster increase of $g_1(t)$ with $t$ holds (similar to the prediction in eq 3). Interpreting then $m(T) = \langle b^2\rangle W^{0.54}$ and using the temperature dependence of the mean-square bond length, which was independently estimated,[51] we obtained $W(T)$ (see Figure 5 below). The temperature dependence of $W(T)$ can be fitted reasonably well by the Vogel−Fulcher law[7]

$$W(T) = W_\infty \exp[-A_w/(T - T_0^{\,w})] \tag{6}$$

with fit parameters $W_\infty = 0.0057$, $A_w = 0.85$, and $T_0{}^w = 0.146$. It is easily shown[51] that neither the Arrhenius law nor the Baessler law[52]

$$W(T) = W_\infty' \exp[-A'/T^2] \tag{7}$$

yield an adequate fit of our data for $W(T)$.

Figure 3 now presents our data for the mean-square displacement of the center of mass

$$g_3(t) = \langle [R_{cm}(t) - R_{cm}(t=0)]^2\rangle \tag{8}$$

Again different regimes can be distinguished. At high temperatures (e.g. $T = 0.4$) $g_3(t)$ shows a subdiffusive behavior for times $t$ for which $g_3(t)$ is clearly smaller than the mean-square gyration radius $\langle R_{gyr}{}^2\rangle$, $g_3(t) \propto t^{x_3}$ with $x_3 \approx 0.75$. For times $t$, for which $g_3(t)$ exceeds $\langle R_{gyr}{}^2\rangle$, we obtain a simple diffusive behavior

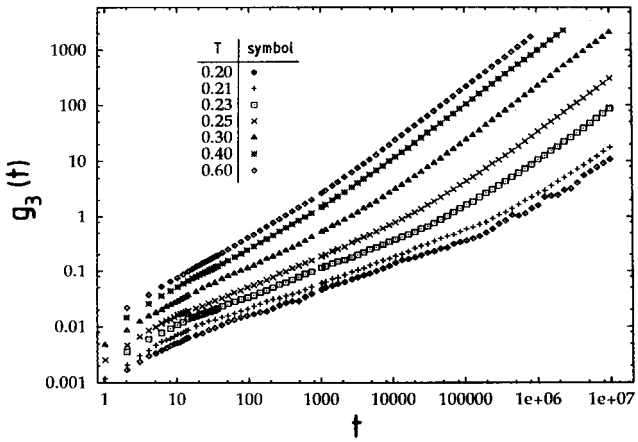


**Figure 3.** Log−log plot of the mean-square displacement of the center of mass $g_3(t)$ vs time $t$, for the same parameters as shown in Figure 2.

$$g_3(t) = 6Dt \tag{9}$$

at large enough times.

Due to eq 9, we estimate the self-diffusion constant $D$ from plotting $g_3(t)/6t$ vs $1/t$, looking for a horizontal plateau at the origin of the plot. In this way the temperature dependence of $D$ could be estimated for $T \geq 0.21$, while for $T \leq 0.20$ no plateau is yet reached even for the largest times, and hence at best upper bounds for $D(T \leq 0.20)$ can be given. Estimates for $D(T)$ are included in Figure 5 below. Again a Vogel−Fulcher fit describes the data reasonably well in the temperature interval $0.23 \leq T \leq 0.40$

$$D(T) = D_\infty \exp[-A_D/(T - T_0^{\,D})] \tag{10}$$

with fit parameters $D_\infty = 0.0027$, $A_D = 0.76$, and $T_0{}^D = 0.129$. It is remarkable that these fit parameters disagree markedly from the parameters obtained by Baschnagel et al.,[39] $D_\infty = 0.00861$, $A_D = 0.396$, and $T_0{}^D = 0.17$. These different fit parameters are due to the fact that Baschnagel et al.[39] used the random hopping algorithm also for equilibration, which restricted the determination of reliable diffusion data to the temperature interval $0.25 \leq T \leq 1.0$. It thus is obvious that the parameters of the Vogel−Fulcher fit depend very sensitively on the temperature interval of the fit, as also was found experimentally.[53] However, the present estimates are for somewhat lower temperatures than used by Baschnagel et al.[39] and therefore should be preferred. Moreover the present estimate for $T_0{}^D$ now is distinctly lower than the estimate for the critical temperature $T_c$ resulting from a fit to modecoupling theory,[54,55] $T_c \approx 0.15$, as it should be.[5,6]

Idealized mode coupling theory (MCT) would represent an alternative to the Vogel−Fulcher analysis, since it predicts a power law dependence of the diffusion coefficient and of relaxation times on temperature. In fact, fitting data in the temperature range $0.25 \leq T \leq 0.40$ to power laws yields fits of acceptable quality, but the resulting critical temperature is unreasonably high, $T_c \approx 0.22$, inconsistent with our data taken at lower temperatures that were not included in this fit. Obviously, such an analysis in terms of power laws is misleading here, since the MCT power law prediction is only valid asymptotically close to $T_c$. The previous analysis[54,55] revealed this asymptotic regime to start at $T = 0.21$ for the present model, outside the range of the above fit, and predicted $T_c \approx 0.15$. On the other hand,

the extended version[28] of MCT (that attempts to include the so-called "hopping processes") implies that very close to $T_c$ these critical singularities are in fact rounded off; therefore, the precise temperature regime where a power law description of our data is appropriate is rather uncertain. Hence a description in terms of power laws is not considered further in the following.

We emphasize that the subdiffusive behavior $g_3(t) \propto t^{x_3}$ (with $x_3 < 1$) mentioned above really is in disagreement with the simple Rouse model, which rather would require that eq 9 holds at all times.[48,49] Actually, the situation becomes worse at lower temperatures, where a crossover occurs from $g_3(t) \propto t^{x_3}$ with $x_3 \approx 0.75$, which then is only seen for very short times ($t \leq 100$ MCS) to a still slower anomalous diffusion with a temperature-dependent exponent {e.g., $x_3(T = 0.27) \approx 0.60$ in this regime while $x_3(T = 0.20) \approx 0.45$}. The time interval over which this extremely slow motion occurs is roughly the same time interval over which one observes a slowing down of the monomer displacements $g_1(t)$ due to the "cage effect". Of course, qualitatively it is clear that during the average "lifetime" of the cages relatively little diffusion is possible, and only on the time scale on which these "cages" have decayed can standard Rouse-like diffusion set in.

These observations are strengthened by a direct comparison of $g_1(t)$ with $g_3(t)$ and with the mean-square displacement $g_2(t)$ of inner monomers in the center of mass system of each chain

$$g_2(t) = \langle [\vec{r}_n(t) - \vec{R}_{cm}(t) - \vec{r}_n(0) + \vec{R}_{cm}(0)]^2 \rangle \quad (11)$$

See Figure 4. At $T = 0.40$, the behavior is typical of the Rouse model:[36,56] $g_1(t) \approx g_2(t)$ until the time where $g_1(t) \approx \langle R_{gyr}{}^2 \rangle$, where $g_2(t)$ starts to level off and ultimately saturates at $\langle R_{gyr}{}^2 \rangle$ as $t \rightarrow \infty$. Note that $g_1(t)$ and $g_3(t)$ merge when $g_1(t) \approx \langle R^2 \rangle$. At $T = 0.23$, this type of behavior is still visible, although now there is a pronounced flattening of all curves on the log−log plot due to the "cage effect". The mean-square displacement $g_1(t) \approx 0.1$ where the onset of this flattening occurs means that many monomers cannot move at all, since the minimum jump distance of a monomer is unity, of course.

At $T = 0.19$, however, the behavior of the mean-square displacements is very anomalous, because for $g_1(t) \geq 0.1$ all displacements $g_1(t)$, $g_2(t)$, and $g_3(t)$ nearly coincide. This means that there is a strong correlation in the motion of the center of mass and of the monomers of the chain. Clearly, Figure 4c is even in qualitative—not just quantitative—disagreement with the basic ideas of the Rouse model, where basically random motions of individual monomers are propagated along the backbone of the chain. These deviations from the simple Rouse description make it also more difficult to extract relaxation times from the mean-square displacements. Following the ideas of Paul et al.,[56] it is convenient to define relaxation times $\tau^{(1)}$, ..., $\tau^{(5)}$ in terms of the following crossing criteria:

$$g_1(t = \tau^{(1)}) = \langle R_{gyr}{}^2 \rangle, \quad g_1(t = \tau^{(2)}) = \langle R^2 \rangle,$$
$$g_3(t = \tau^{(3)}) = \langle R_{gyr}{}^2 \rangle, \quad g_3(t = \tau^{(4)}) = \langle R^2 \rangle,$$
$$g_2(t = \tau^{(5)}) = g_3(t = \tau^{(5)}) \quad (12)$$

The relaxation time $\tau^{(4)}$ is one of the largest relaxation times that can be found in the system, and it can be taken as measuring the Rouse time $\tau_R$, under conditions

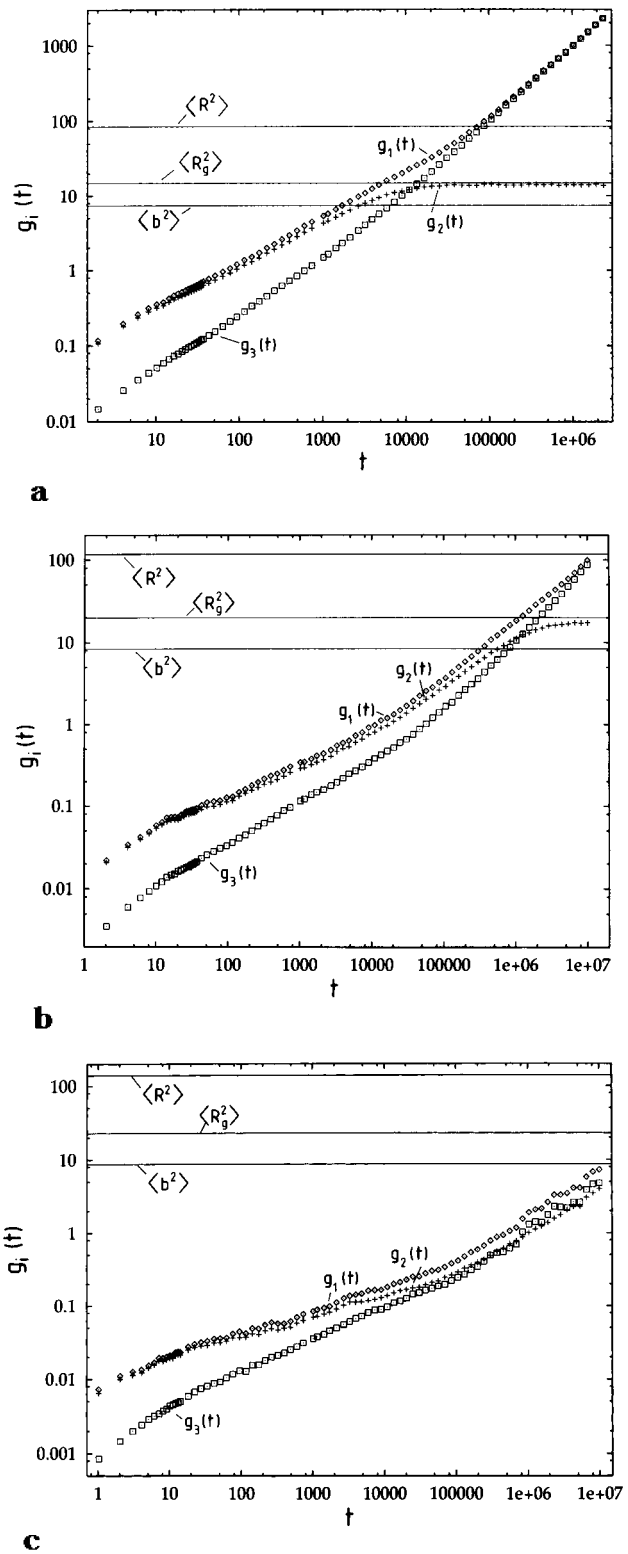


**Figure 4.** Log−log plot of the mean-square displacements $g_1(t)$ (◇), $g_2(t)$ (+) and $g_3(t)$ (□) vs time $t$ at $T = 0.40$ (a) at $T = 0.23$ (b), and at $T = 0.19$ (c). Horizontal straight lines show $\langle R^2 \rangle$ (upper line) $\langle R_g{}^2 \rangle$ (middle line), and $\langle b^2 \rangle$ (lower line).

for which the Rouse model holds. Due to the problems noted in Figure 4, the times defined in eq 12 have been estimated for $T \geq 0.23$ only (Figure 5a). We have also fitted these data by Vogel−Fulcher laws

$$\tau^{(1)} = \tau_\infty{}^{(i)} \exp[A^{(i)}/(T - T_0{}^{(i)})] \quad (13)$$

with $T_0{}^{(i)} = 0.124$, $A^{(1)} = 0.92$, $\tau_\infty{}^{(1)-1} = 0.0053$; $T_0{}^{(2)} =$

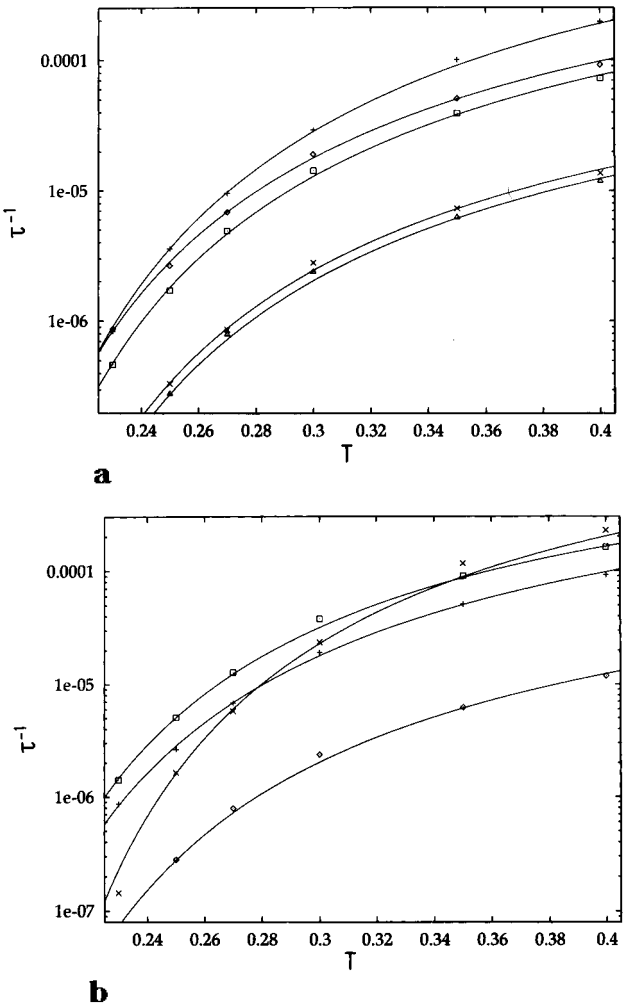


**Figure 5.** Semilog plot of various relaxation times vs temperature. Part a shows the relaxation times $\tau^{(1)}$ defined by eq 12, $\tau^{(1)}$ (◇), $\tau^{(2)}$ (+), $\tau^{(3)}$ (□), $\tau^{(4)}$ (×), and $\tau^{(5)}$ (△), whereas part b compares the temperature dependence of $\tau^{(4)}$ (+) and $\tau^{(5)}$ (◇) with that of the diffusion constant $D$ (□) (see eq 9) and the monomer mobility $W$ (×) (see eq 4). The solid lines are fits to the Vogel−Fulcher equation (see Table 1).

0.124, $A^{(2)} = 0.87$, $\tau_\infty^{(2)-1} = 0.00034$; $T_0^{(3)} = 0.126$, $A^{(3)} = 0.85$, $\tau_\infty^{(3)-1} = 0.0017$; $T_0^{(4)} = 0.124$, $A^{(4)} = 0.88$, $\tau_\infty^{(4)-1} = 0.00030$; $T_0^{(5)} = 0.122$, $A = 0.84$, $\tau_\infty^{(5)-1} = 0.0020$. According to the Rouse model, one expects $\tau^{(1)}$, ..., $\tau^{(5)}$ to be proportional to the Rouse time $\tau_R$ so that their temperature dependence should be the same. In fact, within the error bars, we find $A^{(i)}$ and $T_0^{(i)}$ to be independent of the index $i$, in spite of the difficulties with the Rouse model noted above.

Next, we consider the autocorrelation function of the end-to-end vector $\vec{R}$ defined by

$$\phi_{ete}(t) = \frac{\langle \vec{R}(t)\vec{R}(0)\rangle - \langle \vec{R}(t)\rangle\langle \vec{R}(0)\rangle}{\langle \vec{R}^2(0)\rangle - \langle \vec{R}(0)\rangle^2} \qquad (14)$$

See Figure 6. Figure 6a shows that the relaxation of $\phi_{ete}$ is strongly stretched so that it does not completely decay for $T \le 0.23$ in the studied time window. Despite this strong increase of the polymer relaxation time, the correlation function relaxes in a self-similar fashion, at least at high temperatures $T \ge 0.23$, since all curves in that temperature regime can be shifted onto a common master curve by simply rescaling the time axis with a temperature dependent relaxation time $\tau_{ete}$ (see Figure 6b). This relaxation time was defined as the time at

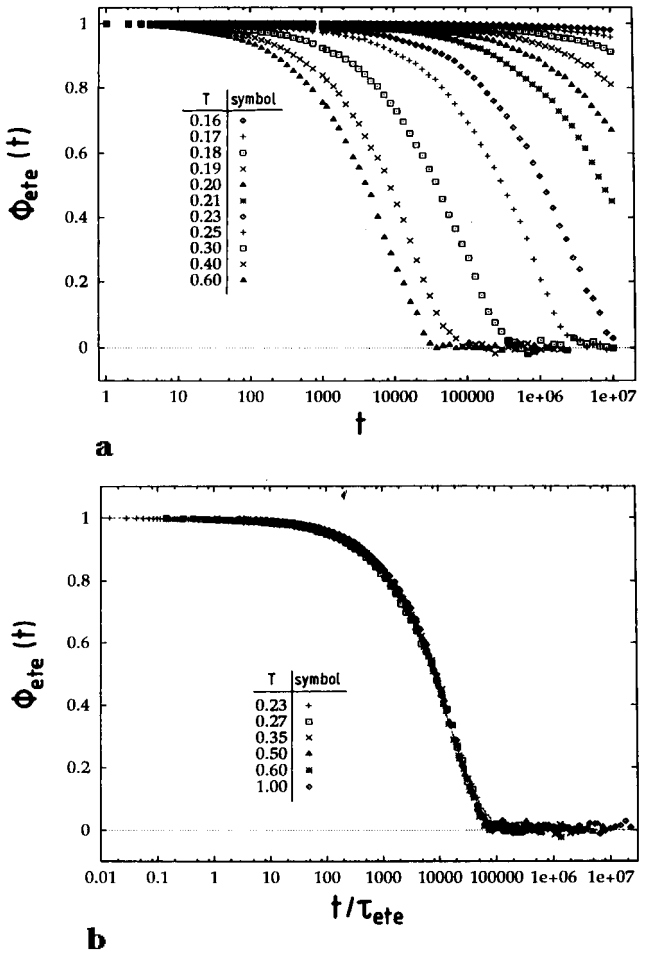


**Figure 6.** (a) Plot of the end-to-end vector correlation function $\phi_{ete}(t)$ vs the logarithm of time, for temperatures from $T = 0.16$ (topmost curve) to $T = 0.60$ (lowest curve). (b) Plot of $\phi_{ete}(t)$ vs the logarithm of the rescaled time $t/\tau_{ete} = t^*$. Equation 15 is included as a dotted line and falls perfectly on the data points apart from a small region near $t^* \approx 10^5$.

which $\phi_{ete}(\tau_{ete}) = 0.2$. The resulting master curve can be rather well described by a Kohlrausch−Williams−Watts stretched exponential function

$$\phi_{ete}(t) = \exp[-(t/\tau_{ete})^y] \qquad y \approx 0.67 \qquad (15)$$

The temperature dependence of $\tau_{ete}$ may be fitted by a Vogel−Fulcher law again; see Figure 14 below. Similar observations were also made for the dynamic behavior of glassy polymer films.[57]

## III. Dynamic Structure Factors

Both the incoherent and the single chain coherent scattering functions, $\phi_q^s(t)$ and $\phi_q^p(t)$, have been evaluated according to the following formulas

$$\phi_q^s(t) = \frac{1}{N}\sum_{n=1}^{N}[\langle \exp[i\vec{q}(\vec{r}_n(t) - \vec{r}_n(0))]\rangle]_q \qquad (16)$$

and

$$\phi_q^s(t) = \frac{1}{N}\sum_{n,m=1}^{N}[\langle \exp[i\vec{q}(\vec{r}_n(t) - \vec{r}_m(0))]\rangle]_q \qquad (17)$$

where $\langle ... \rangle$ denotes the thermodynamic average over all polymers and configurations, as usual, and $[...]_q$ is the spherical average over all $\boldsymbol{q}$ vectors with the same value

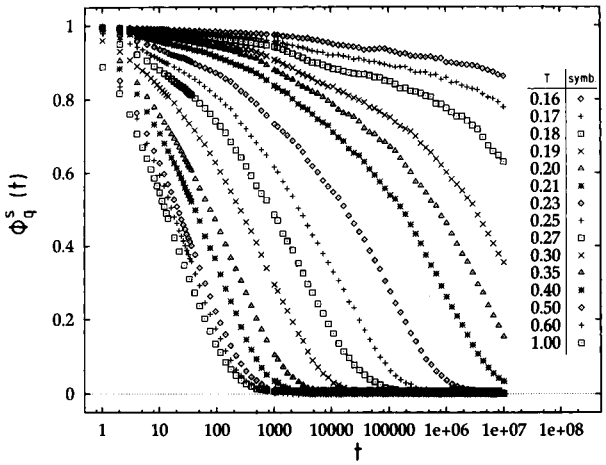


**Figure 7.** Plot of the dynamic intermediate incoherent scattering function $\phi_q^s(t)$ vs time (on a logarithmic scale) for various temperatures as indicated in the figure. The wavenumber is $q = 2.92$, which corresponds to the maximum of the static structure factor.

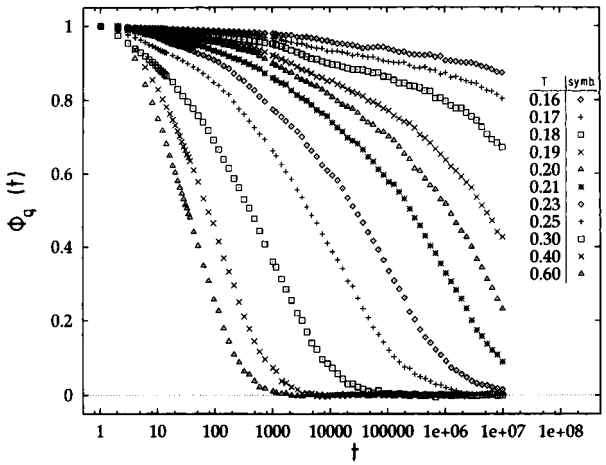


**Figure 8.** Same as Figure 7, but for the single chain coherent scattering function $\phi_q^p(t)$.

$q$. Note that $\phi_q^s(t)$ correlates the position of a monomer $n, \vec{r}_n(t)$, at the time $t$ to its position at time $t = 0$, whereas $\phi_q^p(t)$ also incorporates interference effects between different monomers along the same chain. Figures 7 and 8 show these data for a representative $q$ value, $q = 2.92$, which corresponds to the maximum of the static structure factor.[39]

From the "raw data" in Figures 7 and 8, one can already see rather clearly that the decay of $\phi_q^s(t)$ *and* $\phi_q^p(t)$ is not compatible with a simple relaxation as observed for $\phi_{ete}(t)$, which was described by a *single* stretched exponential function over the whole range. Rather it is obvious that, at temperatures below $T \approx 0.2$, a two-step relaxation process develops: $\phi_q^s(t)$ and $\phi_q^p(t)$ first decay toward a plateau at about $\phi \approx 0.8-0.9$; the lifetime of this plateau strongly increases as the temperature is lowered. Then this plateau decays again with a second relaxation process. Such a two-step relaxation behavior has been predicted by the mode coupling approach to the strutural glass transition for simple liquids.[5,27,28] In refs 54 and 55, it was shown that mode coupling theory can quantitatively account for the decay of $\phi_q^s(t)$ in the intermediate time window of the two-step process. This was interesting due to two reasons: First, the employed polymer model is structurally much more complicated than a simple liquid for which the theory was originally designed. This analysis, therefore, corroborated the theoretical assertion that there are universal features in the dynamics of supercooled liquids, which are largely independent of the microscopic properties of the glass former. Second, a coherent analysis was possible, although the polymer configurations were *not* completely equilibrated. These residual nonequilibrium effects particularly affected the final ($\alpha$) relaxation of $\phi_q^s(t)$ and (presumably also) the temperature dependence of an important theoretical parameter, the so-called "hopping parameter", which triggers the $\alpha$-relaxation close to $T_c$. It would therefore be worthwhile to repeat the analysis for the present completely equilibrated configurations to estimate what the impact of nonequilibrium effects on the theoretical parameters is and to apply the resulting theoretical data to interprete the decay of $\phi_q^s(t)$ at other $q$ values than $q = 2.92$ *and* of $\phi_q^p(t)$. Such an application of mode coupling theory will be done in the future. In the present work, we want to test to what extent the time−temperature superposition principle and the Rouse model hold for $\phi_q^s(t)$ and $\phi_q^p(t)$. Since $\phi_q^s(t)$ and $\phi_q^p(t)$ are qualitatively very similar, we only discuss $\phi_q^s(t)$.

To test the time−temperature superposition we again define a relaxation $\tau(q)$ by requiring $\phi_q^s(t = \tau(q)) = c(q)$, where the constant $c(q)$ has to be chosen such that one has clearly left the first plateau of $\phi_q^s(t)$. E.g., for $q = 2.92$ we choose c(q) = 0.629 to still include $T = 0.18$, since the previous mode coupling analysis showed that temperatures below $T = 0.22$ belong to the asymptotic regime close to $T_c \approx 0.15$. The resulting scaling plot is depicted in Figure 9a. Although there is an approximate collapse of the high-temperature data ($T \geq 0.4$) the results for low temperatures ($T \leq 0.23$) superimpose on a master curve much better. The smaller the temperature, the smaller the rescaled time $t/\tau(q)$ at which the individual $\phi_q^s(t)$ data deviate from the master curve, since $\tau$(q) increases with decreasing temperature and the time window, where $\phi_q^s(t)$ is close to the plateau, extends. Qualitatively, such a behavior is in agreement with mode coupling theory.

Data for other values of $q$ are quite similar[51] and hence are not shown here. Rather we proceed by testing the extent to which our results for $\phi_q^s(t)$ are compatible with the simple Rouse model which predicts[49,58]

$$\phi_q^s(t) = \exp\{-q^2 g_1(t)/6\} \tag{18}$$

Note that eq 18 results from the assumption that the displacements are distributed according to a Gaussian probability distribution; i.e. eq 18 is more general than the Rouse model.

Figure 9b shows a plot of $\phi_q^s(t)$ vs $g_1(t)$, including eq (18). While at high temperatures ($T \geq 0.4$) there is indeed an approximate superposition in a plot of $\phi_q^s(t)$ vs $g_1$, at lower temperatures this superposition holds only for small $g_1$ {namely $g_1 \leq 0.2$} but breaks down for larger $g_1$. The fact that the superposition holds for $q^2 g_1(t)/6 \ll 1$ is trivial, of course, since to first order in $q^2$ the Taylor expansions of eq 16 and eq 18 are identical. But it is interesting to note that deviations from the simple exponential decay (eq 18) actually set in for rather small values of $g_1$ already. Thus even in the high-temperature regime there is some stretching of the relaxation function occurring, due to a distribution of relaxation times. For large $g_1$, dramatic deviations from

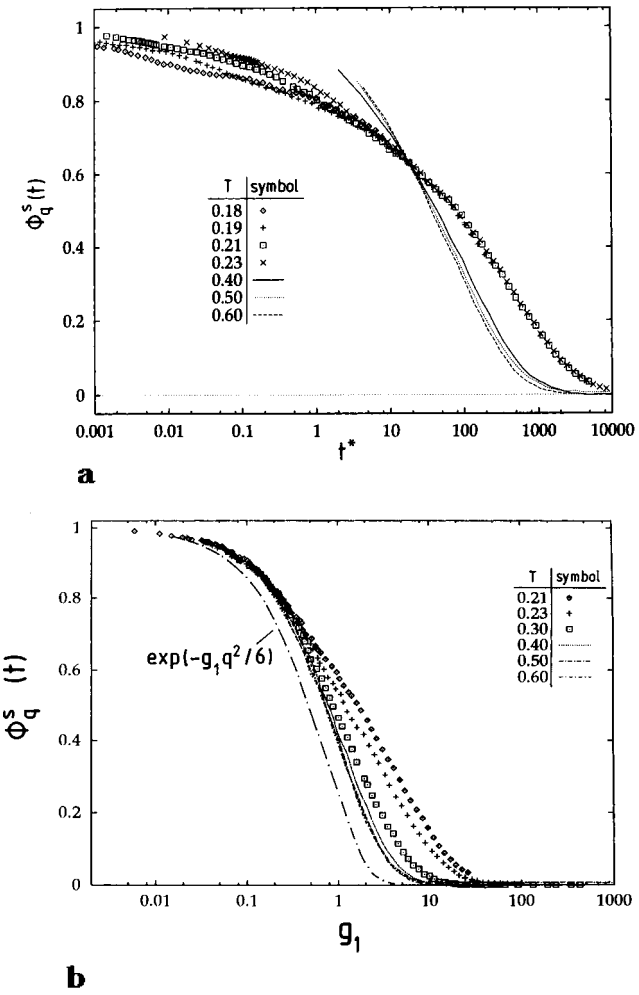


**Figure 9.** (a) Plot of the dynamic incoherent scattering function $\phi_q^s(t)$ vs the rescaled time $t^* = t/\tau(q)$, for $q = 2.92$. For clarity, only four temperatures near the glass transition and three temperatures far above $T_g$ are included. (b) Same data as in part a but plotted vs $g_1(t)$. Equation 18 is included, as indicated.

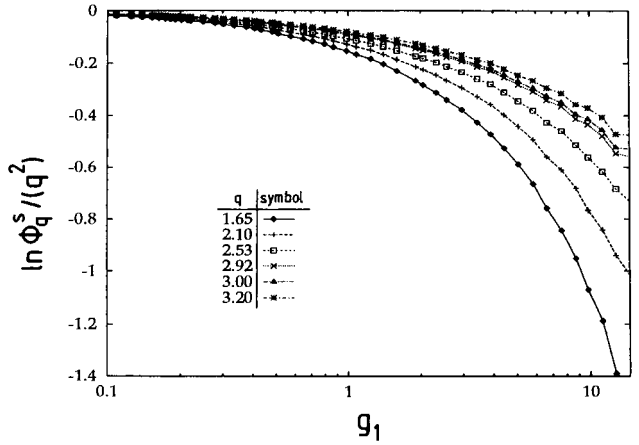


**Figure 10.** Plot of ln $\phi_q^s/q^2$ vs $g_1$, for $T = 0.3$ and six wavenumbers as indicated.

eq 18 occur, as expected. It also must be stressed that for the large wave vectors $\vec{q}$ studied here the simple relation $\ln\phi_q^s(t) \propto q^2$ predicted by eq 18 does not hold either. This behavior is tested in Figure 11 where $\ln\phi_q^s(t)/q^2$ is plotted vs $g_1$. The ***q*** vectors studied clearly splay out rather than collapsing on a master curve. This deviation from the Rouse model is found both at low and at high temperatures.

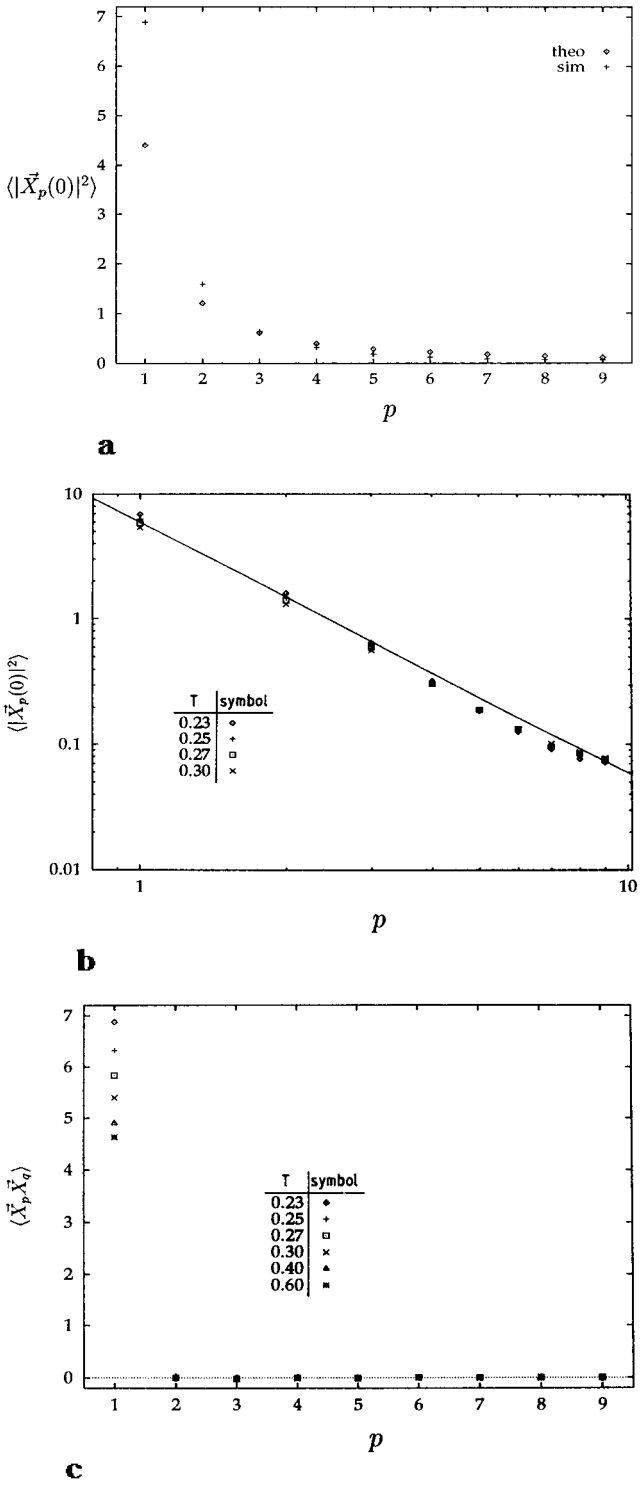


**Figure 11.** (a) Plot of the mean-square amplitude $\langle|\vec{X}_p(0)|^2\rangle$ of the Rouse modes at $T = 0.23$ vs mode index p. Crosses denote the simulation results, while diamonds were calculated from the first line of eq (23) with $l = \langle b^2\rangle^{1/2}$. (b) Log−log plot of $\langle|\vec{X}_p(0)|^2\rangle$ vs $p$ at four temperatures in the supercooled melt regime. Straight line shows eq 23, using $\langle R^2\rangle = 117$ for $T = 0.23$. (c) Static correlation function $\langle\vec{X}_p(0)\vec{X}_p(0)\rangle$ for $q = 1$ plotted vs modes index $p$ for six temperatures as indicated.

## IV. Analysis of the Rouse Modes

In the Rouse model,[48,49,58,59] a chain of $N$ effective monomers connected by harmonic springs is exposed to a medium which exerts friction (and random, uncorrelated forces) on the beads of the chain. As is well-known, a transparent formulation of the dynamics of this model results if one transforms from the dynamics

of the coordinates $\vec{r}_n(t)$ of the $n$th effective monomer to the normal coordinates $\vec{X}_p(t)$

$$\vec{X}_p(t) = \frac{1}{N}\sum_{n=1}^{N} \vec{r}_n(t) \cos\left[\frac{p\pi(n - {}^1/_2)}{N}\right], \quad p = 0, 1, ..., N-1 \quad (19)$$

These normal coordinates are uncorrelated and exhibit a simple exponential decay

$$\langle \vec{X}_p(t)\vec{X}_q(0)\rangle = \delta_{pq}\frac{3k_BT}{\kappa_p}\exp(-t/\tau_p), \quad p = 1, ..., N-1 \quad (20)$$

whereas the zeroth Rouse mode is related to the motion of the center of mass {i.e., to $g_3(t)$}. The amplitude function $\kappa_p$ is expressed in terms of the chain length $N$, the Rouse modes $p$, and an effective bond length $l$ as

$$\kappa_p = \frac{24Nk_BT}{l^2}\sin^2\left[\frac{p\pi}{2N}\right] \xrightarrow{p/N \ll 1} \frac{6\pi^2 k_BT}{Nl^2}p^2 \quad (21)$$

while the relaxation time $\tau_p$ of the individual modes additionally contains the monomer friction coefficient $z$

$$\tau_p = \frac{zl^2}{12k_BT}\left(\sin\left[\frac{p\pi}{2N}\right]\right)^{-2} \xrightarrow{p/N \ll 1} \frac{zN^2l^2}{3\pi^2 k_BTp^2}, \quad p = 1, ..., N-1 \quad (22)$$

In the Rouse model the effective bond length accounts for the short-range interactions along the backbone of the chain. Often, it is taken to be identical to the bond length $\langle b^2\rangle^{1/2}$ of the used polymer model. This is also the point of view adopted in the analysis of the mean-square displacements in section II. Strictly speaking, however, such an identification is only valid for a freely-jointed chain,[49,59] where the persistence length $l_p$ is $\langle b^2\rangle^{1/2}$ so that $\langle R^2\rangle = \langle b^2\rangle(N-1)$, while $\langle R^2\rangle = l_p(T)\langle b^2\rangle^{1/2}(N-1)$ with $l_p(T) > \langle b^2\rangle^{1/2}$ in our case.

In order to test to what extent our model exhibits Rouse-like behavior, we consider the static correlation [see eqs 20−22), for $p > 0$

$$\langle \vec{X}_p(0)\vec{X}_q(0)\rangle = \delta_{pq}\frac{l^2}{8N}\left[\sin\frac{p\pi}{2(N-1)}\right]^{-2} \xrightarrow{p/N \ll 1} \delta_{pq}\frac{Nl^2}{2\pi^2p^2} \quad (23)$$

Figure 11a shows a comparison of the first part of eq 23 with the simulation data for $p = q$ and the choice $l^2 = \langle b^2\rangle$ at $T = 0.23$. Qualitatively, simulation and theory exhibit the same behavior. The static correlation $\langle|\vec{x}_p(0)|^2\rangle$ increases with decreasing $p$ value, but quantitatively the Rouse prediction underestimates this increase. Since $l^2$ appears in the numerator of eq 23, a replacement of $l^2 = \langle b^2\rangle$ by the effective segment length square defined as $l^2 = \langle R^2\rangle/(N-1) > \langle b^2\rangle$ would improve the agreement, e.g., $\langle R^2\rangle = 117.35$ so that $\langle|\vec{x}_p(0)|^2\rangle = 6.66$, which is closer to the simulation data. Using, therefore, $l^2 = \langle R^2\rangle/(N-1)$, Figure 11b tests the continuum approximation (i.e., the second part) of eq 23 for $p = q$ at different temperatures. The figure shows that there is an intermediate regime of $p$ values, where $\langle|\vec{x}_p(0)|^2\rangle \propto p^{-2}$, although our chains are rather short ($N = 10$). This regime expands with increasing temperature (i.e., $p = 2,3$ for $T \le 0.3$ and $p = 2-5$ for $T = 0.4-0.6$), since the corresponding decrease of the persistence length allows the continuum approximation to be applied to smaller distances along the chain backbone. The fact that $l_p > \langle b^2\rangle^{1/2}$ explains the difference between the simulation data and eq 23 at very small $p$ values.

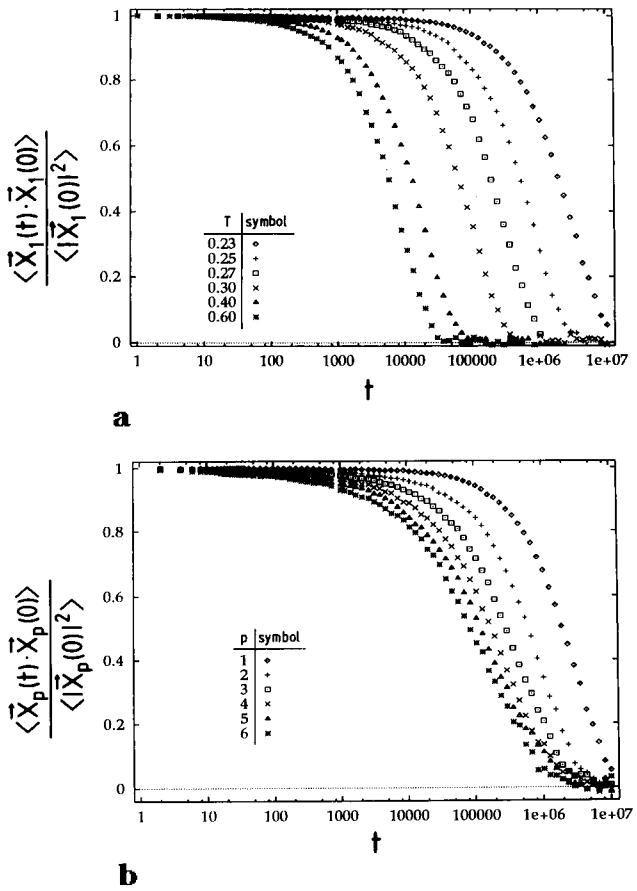


**Figure 12.** (a) Normalized autocorrelation function $\langle \vec{X}_1(t)\vec{X}_1(0)\rangle/\langle|\vec{X}_1(0)|^2\rangle$ of the first Rouse mode plotted vs time for six temperatures as indicated. (b) Normalized autocorrelation function $\langle \vec{X}_p(t)\vec{X}_p(0)\rangle/\langle|\vec{X}_p(0)|^2\rangle$ of the first six Rouse modes at $T = 0.23$ plotted vs time.

A further important prediction of eq 23 is the orthogonality of different Rouse modes. Figure 11c illustrates that, to a very good approximation, static correlations between different Rouse modes indeed vanish (Figure 11c gives an example for $q = 1$; data for higher $q$ ($q = 2.3$) are similar[51]). Thus no nontrivial pair correlations develop in the single-chain configurations of supercooled melts, apart from those picked up by the persistence length.

Since we find that in the framework of the Rouse modes the behavior of the model is unexpectedly close to the theoretical predictions, it is of interest to study the dynamics of the autocorrelation of these modes (Figure 12). Defining a relaxation time $\tau_p$ of the $p$th mode empirically by requiring that $\langle \vec{X}_p(t = \tau_p)\vec{X}_p(0)\rangle/\langle|\vec{X}_p(0)|^2\rangle = 0.4$, we find a very good time−temperature superposition principle (Figure 13a). However, these data clearly deviate from an exponential function, predicted by eq 20—instead the master curves can again be represented by stretched exponentials, as for the end-to-end vector correlation (eq 15). However, a comparison of different modes shows (Figure 13b) that the relaxation functions become the broader the higher the mode index. A possible interpretation of this behavior is that different chains experience different environ-

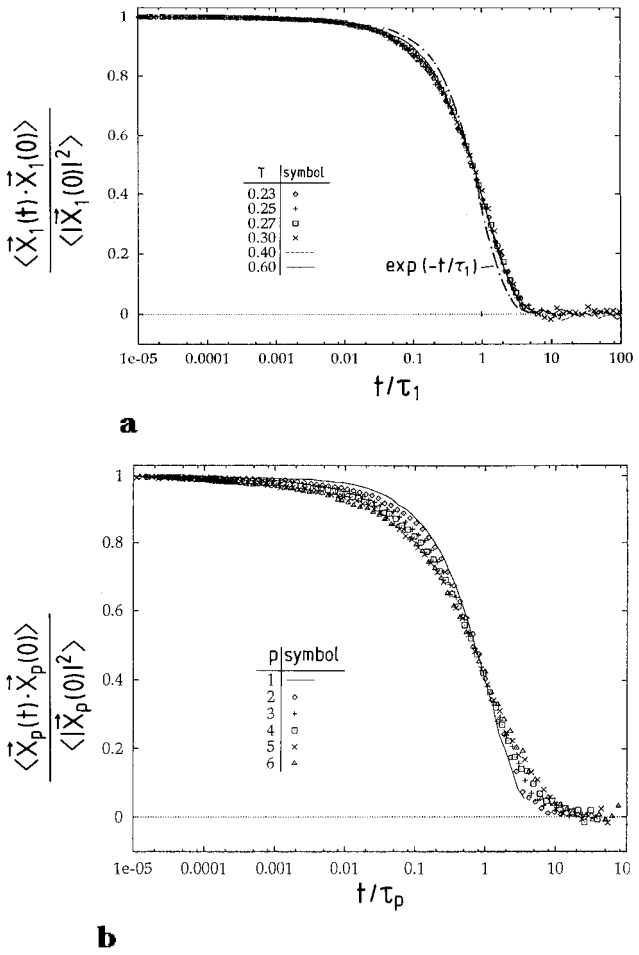


**Figure 13.** (a) Normalized autocorrelation function $\langle \vec{X}_1(t)\vec{X}_1(0)\rangle/\langle|\vec{X}_1(0)|^2\rangle$ of the first Rouse mode plotted vs rescaled time $t^* = t/\tau_1$. Six temperatures are included as indicated. A simple exponential curve is included for comparison. (b) Normalized autocorrelation functions $\langle X_p(t)X_p(0)\rangle/\langle|X_p(0)|^2\rangle$ of the first six Rouse modes plotted vs rescaled time $t^* = t/\tau_p$ at $T = 0.23$.

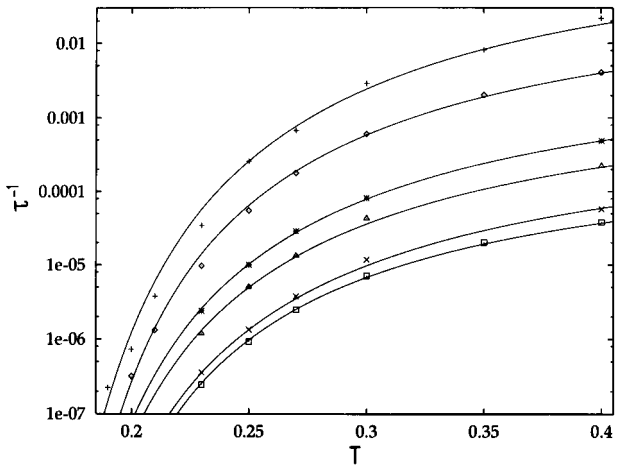


**Figure 14.** Relaxation times $\tau$ plotted vs temperature $\tau(q)$ for $q = 1.65$ (◇) and $q = 3.20$ (+), $\tau_{ete}$ (□) and $\tau_p$ for $p = 1$ (×), $p = 2$ (△) and $p = 3$ (∗). Solid curves show the Vogel−Fulcher fits mentioned in the text.

ments, and this "dynamic heterogeneity"[60] causes a distribution of relaxation times for the Rouse modes. This idea will be explored elsewhere.[60]

Finally, Figure 14 summarizes the temperature dependence of the relaxation times of the first three Rouse modes. For comparison, the time $\tau_{ete}$ and representative times $\tau(q)$ are included. Again one finds that the data

**Table 1. Survey of the Vogel−Fulcher Parameters[a]**

| quantity | fit interval | prefactor | A | $T_0$ |
|---|---|---|---|---|
| W | 0.21−0.40 | 0.0057 | 0.85 | 0.146 |
| D | 0.23−0.40 | 0.0027 | 0.76 | 0.129 |
| $1/\tau^{(1)}$ | 0.23−0.40 | 0.0053 | 0.92 | 0.124 |
| $1/\tau^{(2)}$ | 0.25−0.40 | 0.00034 | 0.87 | 0.124 |
| $1/\tau^{(3)}$ | 0.23−0.40 | 0.0017 | 0.85 | 0.126 |
| $1/\tau^{(4)}$ | 0.25−0.40 | 0.00030 | 0.88 | 0.124 |
| $1/\tau^{(5)}$ | 0.23−0.40 | 0.0020 | 0.84 | 0.122 |
| $1/\tau_{ete}$ | 0.23−0.40 | 0.00065 | 0.768 | 0.132 |
| $1/\tau$ ($q = 1.65$) | 0.20−0.40 | 0.1 | 0.86 | 0.133 |
| $1/\tau$ ($q = 3.2$) | 0.18−0.40 | 0.57 | 0.94 | 0.128 |
| $1/\tau_1$ | 0.23−0.40 | 0.014 | 0.87 | 0.125 |
| $1/\tau_2$ | 0.23−0.40 | 0.048 | 0.85 | 0.127 |
| $1/\tau_3$ | 0.23−0.40 | 0.0115 | 0.86 | 0.128 |

[a] $\tau$ = prefactor × exp[$A/(T - T_0)$], for various relaxation times: monomer mobility $W$ (eq 4), diffusion coefficient $D$ (eq 9), relaxation times $\tau^{(i)}$, $i = 1, ..., 5$ (eq 12), end-to-end vector relaxation time $\tau_{ete}$ (eq 15), scaling time $\tau(q)$ of $\phi_q^s(t)$ at $q = 1.65$, 3.2 [see Section III], and Rouse mode relaxation time $\tau_p$ for $p = 1,2,3$ (Eq 22)

can be well fitted by Vogel−Fulcher laws, $\tau_p = \tau_p^\infty \exp[A_p/(T - T_0^p)]$, with the following parameters: $\tau_1^\infty = 0.014$, $A_1 = 0.87$, $T_0^1 = 0.125$; $(\tau_2^\infty)^{-1} = 0.048$, $A_2 = 0.85$, $T_0^2 = 0.1265$; $\tau_3^\infty = 0.0115$, $A_3 = 0.86$, $T_0^3 = 0.1277$; etc. Again it is gratifying to note that within the accuracy of the fit all $A_i$ are the same and also the $T_0^i$ are the same and moreover in ageement with the Vogel−Fulcher temperatures extracted from the other data, discussed in the previous sections. Note that $\tau_{ete}$ is described by $\tau_{ete} = \tau_{ete}^\infty \exp[A_{ete}/(T - T_0^{ete})]$, with $\tau_{ete}^\infty = 0.00065$, $A_{ete} = 0.768$, and $T_0^{ete} = 0.132$, while the corresponding parameters for $\tau(q = 1.65)$ are $\tau_q^\infty = 0.1$, $A_q = 0.86$, and $T_0^q = 0.133$, and for $q = 3.20$, $\tau_q^\infty = 0.57$, $A_q = 0.94$, and $T_0^q = 0.128$. Thus, although there is a wide variation of the prefactors $\tau^\infty$ over 3 orders of magnitude, all analyzed data yield the parameters $A$ and $T_0$ of the exponential factor in reasonable agreement with each other, as it should be.

## V. Discussion and Some Conclusions

In the present work, we have analyzed the dynamics of monomers and single chains in dense nonentangled polymer melts, studying the effect of temperature variation in the region well above the glass transition of the model. From the analysis of various properties, we conclude that the model has a relatively well-defined Vogel−Fulcher temperature $T_0$ in the range $0.12 \le T_0 \le 0.13$, while previous work[54,55] using mode coupling theory[5,28] had yielded an estimate $T_c \approx 0.15$ for the critical temperature of mode coupling theory. As a consequence, the empirical glass transition temperature $T_g$ (defined by requiring that the largest relaxation time of the system becomes macroscopic, e.g. $\tau_1 = 1$ s, while the simulation time unit is many orders of magnitude smaller, such as 1 MCS = $10^{-11}$ s) should be somewhere in the range $0.13 \le T_g \le 0.15$. The temperature region analyzed here, i.e. mostly the range from $0.2 \le T \le 0.6$, thus roughly would correspond to the region from $T = 1.4T_g$ to $T = 4.2T_g$ in a real experiment; i.e., we probe the region of moderately viscous (slightly supercooled) polymer melts. Note that we use a model on the simple cubic lattice without any attractive intermolecular forces at constant density, and such an approach is clearly too coarse-grained to exhibit a physically meaningful melt to the crystal transition, of course.

Our chain length of $N = 10$ effective monomers (which physically corresponds to a degree of polymerization $N_p \approx 30-50$, since each effective bond comprises $n \approx 3-5$

chemical monomers)[12,14,15,45] is long enough that static properties of chains are very close to Gaussian statistics already (e.g. the single chain structure factor is very well fitted by the Debye formula,[40] etc.) but at the same time short enough that entanglement effects certainly are not present.[36,56] Thus one would naively expect that the dynamics of the chains is well described by the Rouse model, and all what happens is that there is a slowing down due to a temperature-dependent friction coefficient $z(T)$ in the Rouse times $\tau_p$ (eq 22).

However, our simulations yield clear evidence that this picture is far too simple: on the one hand, we do find that the Rouse modes $X_p$ (eq 19) do not develop any significant static correlations among each other, and in this sense they remain well-defined "eigenmodes" of the polymer chains. This observation is consistent with the fact that for all temperatures studied the chains retain their Gaussian properties, although due to the local "stiffening" of the chains (caused by the energetic preference of the "long" bond vector $\vec{b}_0$) the mean-square gyration radius increases from about $\langle R_g^2 \rangle \approx 13$ at high temperatures to about $\langle R_g^2 \rangle \approx 22$ at low temperatures.[39,51] On the other hand, the decay of the Rouse modes is not at all consistent with the simple exponential relaxation, eq 20. Already the first Rouse mode, Figure 12—and the related relaxation function of the end-to-end vector, Figure 6—displays a relaxation with a stretched exponential function rather than a pure exponential, and the stretching of the relaxation functions of the higher Rouse modes becomes even more pronounced; see Figure 13b.

A simple concept to explain the observed behavior is that dynamic heterogeneity[60,61] develops already at the rather high temperatures studied with our model of a polymer melt. The simplest way to include this phenomenon would be to use for each polymer chain an individual friction coefficient $z_{chain}$ and average eq 20 over a suitable distribution function $P(T, z)$ of friction coefficients, thus representing the different environments causing different relaxation rates. However, such a picture is still too simplified, because it cannot explain that the stretching of the relaxation functions increases with increasing mode index $p$.

Instead we have to include a strong variation in effective friction coefficients on the scale of the effective monomer itself, reflecting the fact that more and more effective monomers are temporarily "blocked" in their motions by the "cages" formed in their environment as the temperature is lowered. This "cage effect" is also seen very clearly in the behavior of the mean-square displacements of monomers, of the center of gravity motion, and in the dynamic structure factors.

In the mean-square displacements this effect shows up via intermediate periods of anomalously slow motion ("anomalous diffusion"), at temperatures $T \leq 0.3$, i.e. far above the temperature region where possibly mode coupling theory applies the motions are already significantly hindered.

Of course, it would be of great interest to study temperatures closer to $T_g$. In the present work, we have made every effort to study the dynamics of the model system in (metastable) thermal equilibrium. Since systems that are not well enough equilibrated do show pronounced aging phenomena,[62] the dynamics of relaxation functions[55] and mean-square displacements in not well equilibrated samples is strongly history-dependent and hence even more cumbersome to analyze. We rather feel what is required next is an analytical extension of the Rouse model to deal with the effect of locally different and slowly relaxing environments. Such a description should be a good microscopic starting point for a theory of the dynamics of glassy relaxation in polymers.

**Acknowledgment.** We are thankful for partial support by the Deutsche Forschungsgemeinschaft (DFG) under Grant numbers SFB262/D2, Ba 1554/1-2, and Bi314/12. Stimulating discussions with A. Heuer and W. Paul are acknowledged, as well as generous grants of computing time at the CRAY-YMP computers of the Höchstleistungsrechenzentrum (HLRZ) Jülich and the Regionales Hochschulrechenzentrum Kaiserslautern (RHRK).

## References and Notes

(1) Zallen, R. *The Physics of Amorphous Solids*; Wiley: New York, 1983.
(2) Jäckle, J. *Rep. Progr. Phys.* **1986**, *49*, 171.
(3) McKenna, G. B. In *Comprehensive Polymer Science*; Booth, C., Price, C., Eds.; Pergamon: Oxford, England, 1990; Vol. 2.
(4) Zarzycki, J., Ed. *Materials Science and Technology*, VCH: Weinheim, Germany, 1991; Vol. 9.
(5) Götze, W.; Sjögren, L. *Rep. Progr. Phys.* **1992**, *55*, 241.
(6) Ngai, K. L., Ed. Proceedings of the 2nd International Discussion Meeting on Relaxations in Complex Systems. *J. Non-Cryst. Solids* **1994**, *172−174*.
(7) Vogel, H. *Phys. Z.* **1921**, *22*, 642. Fulcher, G. S. *J. Am. Ceram. Soc.* **1925**, *8*, 339.
(8) Kohlrausch, R. *Ann. Phys. (Leipzig)* **1847**, *12*, 393. Williams, G.; Watts, D. C. *Trans. Faraday Soc.* **1980**, *66*, 80.
(9) Binder, K., Ed. *Monte Carlo Methods in Statistical Physics*; Springer: Berlin, 1979.
(10) Allen, M. P.; Tildesley, J. *Computer Simulation of Liquids*; Oxford University Press: Oxford, England, 1987.
(11) Binder, K., Ed. *The Monte Carlo Method in Condensed Matter Physics*; Springer: Berlin, 1992.
(12) Binder, K., Ed. *Monte Carlo and Molecular Dynamics Simulations in Polymer Science*; Oxford University Press: New York, 1995.
(13) Binder, K., Ciccotti, G., Eds. *Monte Carlo and Molecular Dynamics of Condensed Matter Systems*; Societá Italiana di Física: Bologna, Italy, 1996.
(14) Kremer, K. In ref 13, p 669. Kremer, K. In *Computer Simulations in Chemical Physics*; Allen, M. P., Tildesley, J., Eds.; Kluwer: Dordrecht, The Netherlands, 1993.
(15) Binder K. *Macromol. Chem., Macromol. Symp.* **1991**, *50*, 1.
(16) Brown, D.; Clarke, J. H. R.; Okuda, M.; Yamazaki, T. *J. Chem. Phys.* **1994**, *100*, 1684; *Comput. Phys. Commun.* **1994**, *83*, 1.
(17) Smith, G. D.; Yoon, Y. D. *J. Chem. Phys.* **1994**, *100*, 649.
(18) Paul, W.; Smith, G. D.; Yoon, Y. D. Preprint.
(19) Rigby, D.; Roe, R. J. *J. Chem. Phys.* **1987**, *87*, 7285; **1988**, *89*, 5280; *Macromolecules* **1989**, *22*, 2259.
(20) Takeuchi, H.; Roe, R. J. *J. Chem. Phys.* **1991**, *94*, 7446.
(21) Clarke, J. H. R. In ref 12, Chapter 5.
(22) Angell, C. A.; Clarke, J. H. R.; Woodcock, L. V. *Adv. Chem. Phys.* **1981**, *48*, 397.
(23) Binder, K.; Young, A. P. *Rev. Mod. Phys.* **1986**, *58*, 801.
(24) Binder, K.; Reger, J. D. *Adv. Phys.* **1992**, *41*, 547.
(25) Vollmayr, K.; Kob, W.; Binder, K. *Europhys. Lett.* **1995**, *32*, 715; *J. Chem. Phys.* **1996**, *105*, 4714.
(26) Vollmayr, K.; Kob, W.; Binder, K. *Phys. Rev. B* **1996**, *54*, 15808.
(27) Götze, W. In *Liquids, Freezing and the Glass Transition*; Hansen, J. P., Levesque, D., Zinn-Justin, J., Eds.; North-Holland: Amsterdam, 1990.
(28) Fuchs, M.; Götze, W.; Hildebrand, S.; Latz, A. *J. Phys.: Condens. Matter* **1992**, *4*, 7709.
(29) Gibbs, J. H. *J. Chem. Phys.* **1956**, *25*, 185.
(30) Gibbs, J. H.; DiMarzio, E. A. *J. Chem. Phys.* **1958**, *28*, 373.
(31) DiMarzio, E. A.; Gibbs, J. H. *J. Chem. Phys.* **1958**, *28*, 807.
(32) Adam, G.; Gibbs, J. H. *J. Chem. Phys.* **1965**, *43*, 139.
(33) DiMarzio, E. A.; Gibbs, J. H.; Fleming, P. D., III; Sanchez, I. C. *Macromolecules* **1976**, *9*, 763.
(34) Carmesin, I.; Kremer K. *Macromolecules* **1988**, *21*, 2819.
(35) Deutsch, H. P.; Binder, K. *J. Chem. Phys.* **1991**, *94*, 2249.

(36) Paul, W.; Binder, K.; Heermann, D. W.; Kremer, K. *J. Phys. (Paris) 2* **1991**, *1*, 37.
(37) Wittmann, H.-P.; Kremer, K. *Comput. Phys. Commun.* **1990**, *61*, 309; *ibid* **1992**, *71*, 343.
(38) Wittmann, H. P.; Kremer, K.; Binder, K. *J. Chem. Phys.* **1992**, *96*, 6291.
(39) Baschnagel, J.; Binder, K.; Wittmann, H. P. *J. Phys.: Condens. Matter* **1993**, *5*, 1597.
(40) Baschnagel, J.; Binder, K. *Physica A* **1994**, *204*, 47.
(41) Lobe, B.; Baschnagel, J.; Binder, K. *Macromolecules* **1994**, *27*, 3654.
(42) Wolfgardt, M.; Baschnagel, J.; Binder, K. *J. Phys. (Paris) 2* **1995**, *5*, 1035.
(43) Wolfgardt, M.; Baschnagel, J.; Binder, K. *J. Chem. Phys.* **1995**, *103*, 7166.
(44) Paul, W.; Baschnagel, J. In ref 12, Chapter 6.
(45) Tries, V.; Paul, W.; Baschnagel, J.; Binder, K. *J. Chem. Phys.* **1997**, *106*, 738.
(46) Binder, K. In ref 12, Chapter 1.
(47) Sokal, A. D. In ref 12, Chapter 2.
(48) Rouse, P. E. *J. Chem. Phys.* **1953**, *21*, 127.
(49) Doi, M.; Edwards, S. F. *Theory of Polymer Dynamics*; Clarendon Press: Oxford, England, 1986.
(50) Kremer, K.; Binder, K. *J. Chem. Phys.* **1984**, *81*, 6381.
(51) Okun, K. Diplomarbeit, Johannes Gutenberg-Universität, Mainz, Germany, 1996.
(52) Baessler, H. *Phys. Rev. Lett.* **1987**, *58*, 767.
(53) Stickel, F.; Fischer, E. W.; Richert, R. *J. Chem. Phys.* **1995**, *102*, 6251.
(54) Baschnagel, J. *Phys. Rev. B*, **1994**, *49*, 135.
(55) Baschnagel, J.; Fuchs, M. *J. Phys.: Condens. Matter* **1995**, *7*, 6761.
(56) Paul, W.; Binder, K.; Heermann, D. W.; Kremer, K. *J. Chem. Phys.* **1991**, *95*, 7726.
(57) Baschnagel, J.; Binder, K. *J. Phys. 1 (Fr.)*, **1996**, *6*, 1271.
(58) DeGennes, P. G. *Physics (N.Y.)* **1967**, *3*, 37.
(59) Verdier, P. H.; Stockmayer, W. H. *J. Chem. Phys.* **1962**, *36*, 227.
(60) Heuer, A.; Okun, K. *J. Chem. Phys.*, in press.
(61) Heuer, A.; Wilhelm, M.; Zimmermann, H.; Spiess, H. W. *Phys. Rev. Lett.* **1995**, *75*, 2851.
(62) Baschnagel, J.; Andrejew, E. *Physica* **1996**, *A233*, 117.

MA961605B